Optical properties of metallic films for vertical-cavity optoelectronic devices

Aleksandar D. Rakić, Aleksandra B. Djurišić, Jovan M. Elazar, and Marian L. Majewski

We present models for the optical functions of 11 metals used as mirrors and contacts in optoelectronic and optical devices: noble metals (Ag, Au, Cu), aluminum, beryllium, and transition metals (Cr, Ni, Pd, Pt, Ti, W). We used two simple phenomenological models, the Lorentz–Drude (LD) and the Brendel–Bormann (BB), to interpret both the free-electron and the interband parts of the dielectric response of metals in a wide spectral range from 0.1 to 6 eV. Our results show that the BB model was needed to describe appropriately the interband absorption in noble metals, while for Al, Be, and the transition metals both models exhibit good agreement with the experimental data. A comparison with measurements on surface normal structures confirmed that the reflectance and the phase change on reflection from semiconductor–metal interfaces (including the case of metallic multilayers) can be accurately described by use of the proposed models for the optical functions of metallic films and the matrix method for multilayer calculations. © 1998 Optical Society of America

OCIS codes: 160.4760, 310.6860, 160.3380, 250.7260.

1. Introduction

It is well known that the performances of optoelectronic devices are strongly influenced by the choice of their ohmic contacts. Recently semiconductor lasers and light-emitting diodes with metallic mirrors have received much attention.

In vertical-cavity-surface-emitting lasers (VCSEL's) a metallic layer is commonly deposited on top of a semiconductor distributed Bragg reflector (DBR) mirror to increase the reflectivity of the mirror and to serve as a contact.[1–5] Asymmetric cladding separate confinement heterostructure lasers rely on the surface metal to form an adequate waveguide for transverse confinement of the optical mode. Consequently, the modal properties are a strong function of the choice of metals (and metal thickness) for the *p*-type contact.[6–8] Metallic layers are not only interesting for lasers, they are also useful in a new generation of optical devices called resonant-cavity light-emitting diodes (RCLED's). The RCLED's have structures similar to VCSEL's, but they require mirror reflectivity of only 90–95%. This reflectivity can be achieved by using the metallic layer instead of the technologically more involved semiconductor DBR mirror. RCLED's have been demonstrated with either one[9–11] or both metallic mirrors.[12,13] The RC scheme was also successfully applied to photodetectors with metallic (Ag, Al) mirrors.[14,15]

In all cases the needed high mirror reflectivity can be attained by using pure noble metals or Al, whereas the good ohmic contact and reliable adhesion are achieved by using layers of wetting metals (Ti, Pd, Cr) between the semiconductor and the high-reflectivity metal layer. For metal/GaAs ohmic contacts, the preferred metal is usually Au. Unfortunately, a pure Au contact has two major disadvantages; it has very poor adhesion and it diffuses rapidly into the semiconductor. To rectify these shortcomings of a *p*-type semiconductor/Au contact, a thin layer of Ti is usually employed to improve adhesion, while the thin layer of Pt serves as a diffusion barrier.[6] Several other metallization schemes for GaAs devices are also in use: nonalloyed AuZn/Au for *p*-type ohmic contact and alloyed AuGe/Ni/Au for *n*-type ohmic contact,[13] Ag/Au/Ti/Au for *p*-type and AuGe for *n*-type contact,[10] Ag/CdSnO for *p*-type semitransparent contacts.[11] The metal/InP ohmic contact design concepts are very similar to those suggested for metal/GaAs systems. Traditionally, Au-based alloy contacts (AuZn, AuZnNi, AuBe, AuGe, AuNi, AuCr, AuCd, AuMg, AuMn) have been used as well as nonalloyed Ti/Pt/Au and Ti/Au metallization schemes for both contacts.[14,16,17] How-

A. D. Rakić and M. L. Majewski are with the Department of Computer Science and Electrical Engineering, The University of Queensland, Brisbane QLD 4072, Australia. A. B. Djurišić and J. M. Elazar are with the Faculty of Electrical Engineering, University of Belgrade, P.O. Box 816, Belgrade, Yugoslavia.

Received 22 December 1997.
0003-6935/98/225271-13$15.00/0

ever, nonalloyed composite coatings are much preferred when contact serves also as part of the optical cavity. Materials such as W and W alloys are certainly suitable candidates for obtaining abrupt metal–semiconductor interfaces. Pure gold contacts, acting at the same time as semitransparent mirrors, have been found suitable for CdHgTe and CdZnTe devices.[9]

Because metallic mirrors are the elements of the resonant cavity of VCSEL's and RCLED's, it is necessary to determine precisely the phase and the amplitude of the reflection coefficient of such a metal–semiconductor interface to design the resonator properly. Taking into account the phase change on reflection on the metal–semiconductor interface enables one to calculate the thickness of the last semiconductor layer (the phase-matching layer) before the metal to match the phase characteristic of DBR at the design wavelength. The phase change on reflection at the metal–semiconductor interface in the near-IR and visible wavelength range is always less than 180°. Furthermore it can be a very sensitive function of wavelength in the vicinity of interband transitions of the employed metal (see, for example, Ref. 18 and references therein).

The amplitude and the phase of the reflection coefficient can be calculated from the optical constants [refractive index $n(\omega)$ and extinction coefficient $k(\omega)$] or from the complex optical dielectric function $\epsilon_r(\omega) = \epsilon_{r1}(\omega) - i\epsilon_{r2}(\omega)$. Often models for $\epsilon_r(\omega)$ that are closely related to the electronic band structure prove to be exceedingly complicated for practical use or are restricted to a certain material. For example, one can express the bulk film optical dielectric function of Al by using the Ashcroft and Sturm model.[19] In contrast, the optical functions of the noble metals are not amenable to such interpretation. Therefore simple phenomenological models such as the Lorentz-Drude (LD) oscillator model[20] or Erman's model,[21] based on the damped harmonic oscillator approximation, which can be used to describe optical properties of an arbitrary solid, are still frequently used.[22–24] Although there are several compilations of the optical properties of metals,[25–30] authors know of no systematic parameterization, other than studies in which the free-electron Drude model was used, which is not adequate in the near-IR and the visible wavelength range. Therefore there is need for a study that would provide a description of the optical functions of metals in terms of a simple model and that would cover all the metals used for optoelectronic applications.

We present parameterization of the large number of metals for optoelectronic applications, using (a) a simple LD model and (b) a recent model by Brendel and Bormann[31] (BB). We also give a new derivation of this flexible phenomenological model and present a BB model in two different analytic forms suitable for implementation on a computer. Therefore the purpose of this paper is twofold: (a) to present a comprehensive and accurate parameterization of the optical properties of metals for optoelectronic applications in a wide spectral range and (b) to compare the LD model with the new BB model on several examples.

In Section 2 we describe the LD and the BB models. In Section 3 we give an overview of the optical dielectric functions of the metals used in this study and provide parameterizations of these optical functions in terms of LD and BB models. In Section 4 we compare our results with recent measurements performed on vertical cavity structures. In Appendix A we outline the derivation of our analytic form of the BB model.

2. Material Models

A. Lorentz–Drude Model

First we briefly discuss the LD model often used for parameterization of the optical constants of metals.[18,32–34] It has been shown[35,36] that a complex dielectric function $\epsilon_r(\omega)$ can be expressed in the following form:

$$\hat{\epsilon}_r(\omega) = \hat{\epsilon}_r^{(f)}(\omega) + \hat{\epsilon}_r^{(b)}(\omega), \tag{1}$$

which separates explicitly the intraband effects (usually referred to as free-electron effects) from interband effects (usually referred to as bound-electron effects). The intraband part $\hat{\epsilon}_r^{(f)}(\omega)$ of the dielectric function is described by the well-known free-electron or Drude model[37,38]:

$$\hat{\epsilon}_r^{(f)}(\omega) = 1 - \frac{{\Omega_p}^2}{\omega(\omega - i\Gamma_0)}. \tag{2}$$

The interband part of the dielectric function $\hat{\epsilon}_r^{(b)}(\omega)$ is described by the simple semiquantum model resembling the Lorentz result for insulators:

$$\hat{\epsilon}_r^{(b)}(\omega) = \sum_{j=1}^{k} \frac{f_j {\omega_p}^2}{({\omega_j}^2 - \omega^2) + i\omega\Gamma_j}, \tag{3}$$

where ω_p is the plasma frequency, k is the number of oscillators with frequency ω_j, strength f_j, and lifetime $1/\Gamma_j$, while $\Omega_p = \sqrt{f_0}\omega_p$ is the plasma frequency associated with intraband transitions with oscillator strength f_0 and damping constant Γ_0.

B. Brendel–Bormann Model

Let us now concentrate on the interband part $\hat{\epsilon}_r^{(b)}(\omega)$ of the dielectric function. Usually the Lorentz model employs oscillators at major critical points (CP's) in the joint density of states that correspond to interband transition energies $\hbar\omega_j$, with some additional oscillators to model absorption between CP's. It has been shown,[39,40] however, that usually the Gaussian line shape is a much better approximation for the broadening function than the Lorentzian line shape. If the same strength and full width at half-maximum are assumed for both absorption line shapes, the Lorentzian broadening function has higher and more extended wings compared with the Gaussian one. Accordingly, all the models based on the Lorentzian broadening function exhibit excessive absorption far from the CP's. Recently, Brendel and

Bormann[31] have proposed a model for a dielectric function of solids that replaces a Lorentz oscillator with a superposition of an infinite number of oscillators, given by

$$\chi_j(\omega) = \frac{1}{\sqrt{2\pi}\sigma_j}\int_{-\infty}^{+\infty}\exp\left[-\frac{(x-\omega_j)^2}{2\sigma_j^2}\right] \times \frac{f_j\omega_p^2}{(x^2-\omega^2)+i\omega\Gamma_j}\,dx. \quad (4)$$

The number of harmonic oscillators per frequency interval is determined by a Gaussian function. In their original paper[31] the authors suggested that the model is applicable to an amorphous solid in the far-IR part of the spectrum and constructed the model from a phenomenological point of view. However, we show that this model can be used to describe optical properties of a wide range of materials including metals. Integral (4) can be solved analytically (see Appendix A) to obtain

$$\chi_j = \frac{i\sqrt{\pi}\,f_j\omega_p^2}{2\sqrt{2}a_j\sigma_j}\left[w\left(\frac{a_j-\omega_j}{\sqrt{2}\sigma_j}\right)+w\left(\frac{a_j+\omega_j}{\sqrt{2}\sigma_j}\right)\right], \quad (5)$$

where $a_j = a_j' + ia_j'' = (\omega^2 - i\omega\Gamma_j)^{1/2}$ and $a_j'' > 0$, while $w(z)$ is the error integral of the complex argument, defined by [see Ref. 41, Eq. (7.1.3)]

$$w(z) = e^{-z^2}\,\mathrm{erfc}(-iz) \qquad (\mathrm{Im}[z] > 0), \quad (6)$$

and $\mathrm{erfc}(z)$ is the complementary error function,

$$\mathrm{erfc}(z) = \frac{2}{\sqrt{\pi}}\int_z^{+\infty}\exp(-t^2)dt. \quad (7)$$

A solution satisfying the condition $a_j'' > 0$ is

$$a_j' = \frac{\omega}{\sqrt{2}}\{[1+(\Gamma_k/\omega)^2]^{1/2}+1\}^{1/2},$$

$$a_j'' = \frac{\omega}{\sqrt{2}}\{[1+(\Gamma_k/\omega)^2]^{1/2}-1\}^{1/2}. \quad (8)$$

We suggest that Eq. (5) also be expressed in terms of confluent hypergeometric functions, namely, the Kummer functions of the second kind $U(a, b, z)$. By employing the relation between $\mathrm{erfc}(z)$ and $U(a, b, z)$ [cf. Ref. 41, Eq. (13.6.39)],

$$U(1/2, 1/2, z^2) = \sqrt{\pi}e^{z^2}\,\mathrm{erfc}(z), \quad (9)$$

we obtain

$$\chi_j = \frac{if_j\omega_p^2}{2\sqrt{2}a_j\sigma_j}\left\{U\left[1/2, 1/2, -\left(\frac{a_j-\omega_j}{\sqrt{2}\sigma_j}\right)^2\right] + U\left[1/2, 1/2, -\left(\frac{a_j+\omega_j}{\sqrt{2}\sigma_j}\right)^2\right]\right\}. \quad (10)$$

When we keep in mind that special functions of complex arguments are now readily available through languages such as Mathematica,[42] or from various Fortran and C libraries, this model is as easy to implement as a simple LD model. The expression for the complete optical dielectric function now reads

$$\hat{\epsilon}_r(\omega) = 1 - \frac{\Omega_p^2}{\omega(\omega - i\Gamma_0)} + \sum_{j=1}^{k}\chi_j(\omega), \quad (11)$$

where k is the number of BB oscillators used to interpret the interband part of the spectrum. Thus an analytic function is obtained that satisfies the Kramers–Kronig (K–K) relations and has a flexible shape of the absorption profile. This function, however, introduces an additional parameter per each transition besides the strength, energy, and linewidth. This additional parameter σ allows for a continuous change in the absorption line shapes ranging from a purely Lorentzian for $\sigma_j \approx 0$ to a nearly Gaussian for $\Gamma_j \approx 0$. Therefore a range of absorption function approximations with similar kernels and different wings can be obtained with Eq. (11).

C. Optical Constants and Reflectivity

Refractive index n and extinction coefficient k, being the real and the imaginary parts of the complex refractive index $\hat{N} = n - ik$, can be calculated from the complex optical dielectric function:

$$n = \frac{1}{\sqrt{2}}[(\epsilon_{r1}^2 + \epsilon_{r2}^2)^{1/2} + \epsilon_{r1}]^{1/2},$$

$$k = \frac{1}{\sqrt{2}}[(\epsilon_{r1}^2 + \epsilon_{r2}^2)^{1/2} - \epsilon_{r1}]^{1/2}. \quad (12)$$

For the simple semiconductor–metal interface, normal incidence reflectivity can be calculated by use of[43]

$$R = \frac{(n_0-n_1)^2 + k_1^2}{(n_0+n_1)^2 + k_1^2}, \quad (13)$$

where the phase shift associated with the reflected beam is[43]

$$\varphi = \arctan\frac{2n_0k_1}{(n_0^2 - n_1^2 - k_1^2)} \quad (14)$$

and where n_0 is the refractive index of the incident medium (semiconductor) and $\hat{N}_1 = n_1 - ik_1$ is the refractive index of the substrate (metal). Equations (13) and (14) imply that the incident medium is lossless owing to the well-known problems of defining reflectivity for the wave incident from the lossy medium.[43] However, the amplitude reflection coefficient and the phase are well defined, and there are no problems in calculating the phase shift upon reflection needed in resonator design, even if the lossy incident medium (semiconductor) is assumed.[43,44]

3. Results for 11 Metals

We have parameterized 11 most frequently used metals: noble metals (Ag, Au, and Cu), aluminum, beryllium, and some of the transition metals (Cr, Ni, Pd, Pt, Ti, and W). For all the metals we have carefully chosen relevant optical data, trying always to engage

Table 1. Values of the Plasma Frequencies $\hbar\omega_p$ (eV)

Metal	$\hbar\omega_p$
Ag	9.01
Au	9.03
Cu	10.83
Al	14.98
Be	18.51
Cr	10.75
Ni	15.92
Pd	9.72
Pt	9.59
Ti	7.29
W	13.22

the measurements obtained on films similar (in terms of geometry, morphology, and the process of growth) to the films used in optoelectronic devices. Also, wherever possible, we used K–K consistent sets of optical data in the whole range. To fit the models (LD and BB) to the data, we employed the following objective function:

$$\chi^2 = \sum_{i=1}^{i=N} \left[\left| \frac{\epsilon_{r1}(\omega_i) - {\epsilon_{r1}}^{\exp}(\omega_i)}{{\epsilon_{r1}}^{\exp}(\omega_i)} \right| + \left| \frac{\epsilon_{r2}(\omega_i) - {\epsilon_{r2}}^{\exp}(\omega_i)}{{\epsilon_{r2}}^{\exp}(\omega_i)} \right| \right]^2. \tag{15}$$

To minimize the merit (or cost) function, we use the acceptance-probability-controlled simulated annealing algorithm (described in detail in Refs. 32 and 34), which was specifically designed for solving parameter estimation problems. The algorithm has two independent features that make it superior to other simulated annealing algorithms in terms of convergence rate and robustness: first, the replacement of the temperature control of the cooling schedule with direct control of acceptance probability; second, the highly efficient move generation mechanism. This algorithm has proved to be insensitive to initial parameter values and extremely efficient in escaping local minima. No attempt has been made here to constrain the values of the oscillator strengths and linewidths in the fitting procedure, even by an order of magnitude. Optimal values for LD model parameters, obtained by this algorithm, are given in Table 2, whereas Table 3 presents optimal parameters for the BB model. The values for oscillator strengths correspond to the plasma frequencies $\hbar\omega_p$ given in Table 1.

A. Silver

For parameterization of the optical constants of silver, we used the data tabulated in Ref. 45. This composite set consists of the polarimetric data of Dold and Mecke[46] between 0.125 and 0.98 eV, polarimetric measurements of Winsemius *et al.*[47] between 0.65 and 3.3 eV, and K–K analyzed *in situ* reflectance measurements of Leveque *et al.*[48] from 3.3 to 26.5 eV. For our fits we used data between 0.125 and 6 eV.

The data of Leveque *et al.*[48] and of Winsemius *et al.*[47] agree well at ~3.4 eV where they meet. The dispersion data (ϵ_{r1}) of Dold and Mecke[46] have the same slope but slightly lower values than the data of Winsemius *et al.*[47] in the region of overlap (0.65–1 eV). The absorption data (ϵ_{r2}) of the same groups continue well at ~1 eV with a somewhat steeper slope in the data of Winsemius *et al.*[47] Our model dielectric function agrees well in slope and magnitude with both data sets, as depicted in Fig. 1.

B. Gold

Gold has been the subject of extensive optical studies. Of particular interest to our application is the study of Thèye[49] providing the dielectric function of Au in the 0.5–6-eV range from the measurements of the reflectance and the transmittance of semitransparent

Table 2. Values of the LD Model Parameters

	Metal										
Parameters	Ag	Au	Cu	Al	Be	Cr	Ni	Pd	Pt	Ti	W
f_0	0.845	0.760	0.575	0.523	0.084	0.168	0.096	0.330	0.333	0.148	0.206
Γ_0	0.048	0.053	0.030	0.047	0.035	0.047	0.048	0.008	0.080	0.082	0.064
f_1	0.065	0.024	0.061	0.227	0.031	0.151	0.100	0.649	0.191	0.899	0.054
Γ_1[a]	3.886	0.241	0.378	0.333	1.664	3.175	4.511	2.950	0.517	2.276	0.530
ω_1[a]	0.816	0.415	0.291	0.162	0.100	0.121	0.174	0.336	0.780	0.777	1.004
f_2	0.124	0.010	0.104	0.050	0.140	0.150	0.135	0.121	0.659	0.393	0.166
Γ_2	0.452	0.345	1.056	0.312	3.395	1.305	1.334	0.555	1.838	2.518	1.281
ω_2	4.481	0.830	2.957	1.544	1.032	0.543	0.582	0.501	1.314	1.545	1.917
f_3	0.011	0.071	0.723	0.166	0.530	1.149	0.106	0.638	0.547	0.187	0.706
Γ_3	0.065	0.870	3.213	1.351	4.454	2.676	2.178	4.621	3.668	1.663	3.332
ω_3	8.185	2.969	5.300	1.808	3.183	1.970	1.597	1.659	3.141	2.509	3.580
f_4	0.840	0.601	0.638	0.030	0.130	0.825	0.729	0.453	3.576	0.001	2.590
Γ_4	0.916	2.494	4.305	3.382	1.802	1.335	6.292	3.236	8.517	1.762	5.836
ω_4	9.083	4.304	11.18	3.473	4.604	8.775	6.089	5.715	9.249	19.43	7.498
f_5	5.646	4.384	—	—	—	—	—	—	—	—	—
Γ_5	2.419	2.214	—	—	—	—	—	—	—	—	—
ω_5	20.29	13.32	—	—	—	—	—	—	—	—	—

[a]In electron volts.

Table 3. Values of the BB Model Parameters

Parameter	Metal										
	Ag	Au	Cu	Al	Be	Cr	Ni	Pd	Pt	Ti	W
f_0	0.821	0.770	0.562	0.526	0.081	0.154	0.083	0.330	0.333	0.126	0.197
Γ_0	0.049	0.050	0.030	0.047	0.035	0.048	0.022	0.009	0.080	0.067	0.057
f_1	0.050	0.054	0.076	0.213	0.066	0.338	0.357	0.769	0.186	0.427	0.006
$\Gamma_1{}^a$	0.189	0.074	0.056	0.312	2.956	4.256	2.820	2.343	0.498	1.877	3.689
$\omega_1{}^a$	2.025	0.218	0.416	0.163	0.131	0.281	0.317	0.066	0.782	1.459	0.481
$\sigma_1{}^a$	1.894	0.742	0.562	0.013	0.277	0.115	0.606	0.694	0.031	0.463	3.754
f_2	0.133	0.050	0.081	0.060	0.067	0.261	0.039	0.093	0.665	0.218	0.022
Γ_2	0.067	0.035	0.047	0.315	3.962	3.957	0.120	0.497	1.851	0.100	0.277
ω_2	5.185	2.885	2.849	1.561	0.469	0.584	1.059	0.502	1.317	2.661	0.985
σ_2	0.665	0.349	0.469	0.042	3.167	0.252	1.454	0.027	0.096	0.506	0.059
f_3	0.051	0.312	0.324	0.182	0.346	0.817	0.127	0.309	0.551	0.513	0.136
Γ_3	0.019	0.083	0.113	1.587	2.398	2.218	1.822	2.022	2.604	0.615	1.433
ω_3	4.343	4.069	4.819	1.827	2.827	1.919	4.583	2.432	3.189	0.805	1.962
σ_3	0.189	0.830	1.131	0.256	1.446	0.225	0.379	1.167	0.766	0.799	0.273
f_4	0.467	0.719	0.726	0.014	0.311	0.105	0.654	0.409	2.214	0.0002	2.648
Γ_4	0.117	0.125	0.172	2.145	3.904	6.983	6.637	0.119	2.891	4.109	4.555
ω_4	9.809	6.137	8.136	4.495	4.318	6.997	8.825	5.987	8.236	19.86	5.442
σ_4	1.170	1.246	1.719	1.735	0.893	4.903	0.510	1.331	1.146	2.854	1.912
f_5	4.000	1.648	—	—	—	—	—	—	—	—	—
Γ_5	0.052	0.179	—	—	—	—	—	—	—	—	—
ω_5	18.56	27.97	—	—	—	—	—	—	—	—	—
σ_5	0.516	1.795	—	—	—	—	—	—	—	—	—

[a]In electron volts.

films of various thicknesses. A detailed analysis of these samples indicated that it is possible to produce very thin but continuous films with the same properties as the bulk material. The results on well-crystallized films of thicknesses from 10 to 25 nm evaporated in ultrahigh vacuum (10^{-11} Torr) show good agreement with data obtained on bulk samples.[49]

In our analysis we used the ellipsometric data of Dold and Mecke[46] in the 0.125–0.98-eV region and the data of Thèye[49] between 1.0 and 6.0 eV. Both data sets were tabulated in Ref. 45. Figure 2 shows the real and the imaginary part of the dielectric function of gold versus photon energy between 0.2 and 5 eV. At ~2 eV, where the lowest-laying interband transitions occur in Au, the BB model fits the data much better than the LD model. This better set can

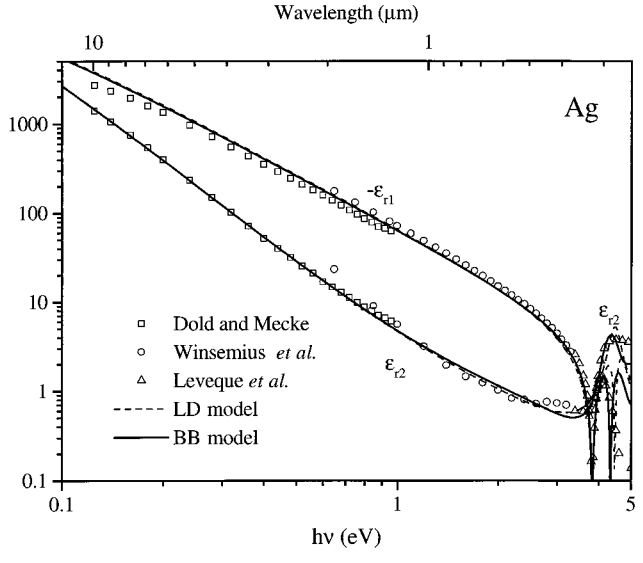

Fig. 1. Real and imaginary parts of the optical dielectric function of Ag: solid curves, values that we calculated using the BB model; dashed curves, the LD model. Also shown are the selected experimental data points from Dold and Mecke,[46] Winsemius *et al.*,[47] and Leveque *et al.*[48]

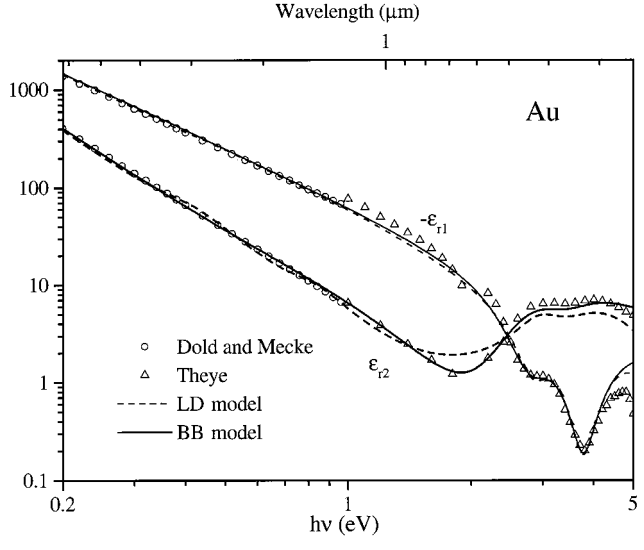

Fig. 2. Real and imaginary parts of the optical dielectric function of Au: solid curves, values that we calculated using the BB model; dashed curves, the LD model. Also shown are selected experimental data points from Dold and Mecke[46] and Thèye.[49]

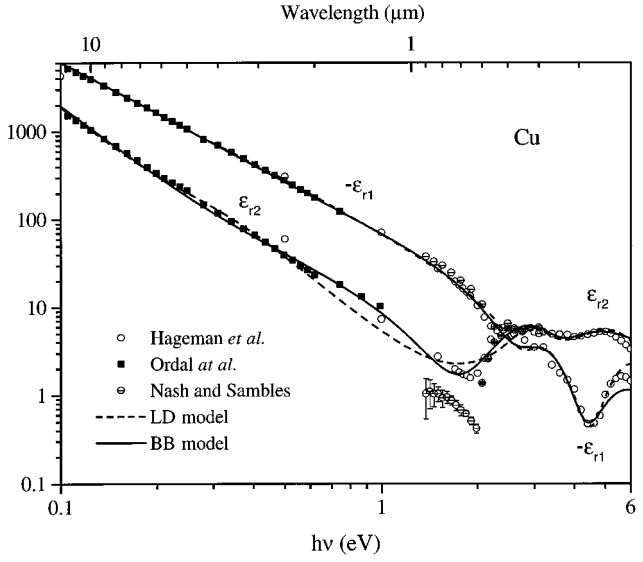

Fig. 3. Real and imaginary parts of the optical dielectric function of Cu: solid curves, values calculated by use of the BB model; dashed curves, LD model. Also shown are tabulated data from Hagemann *et al.*,[50] Ordal *et al.*,[26] and Nash and Sambles.[54]

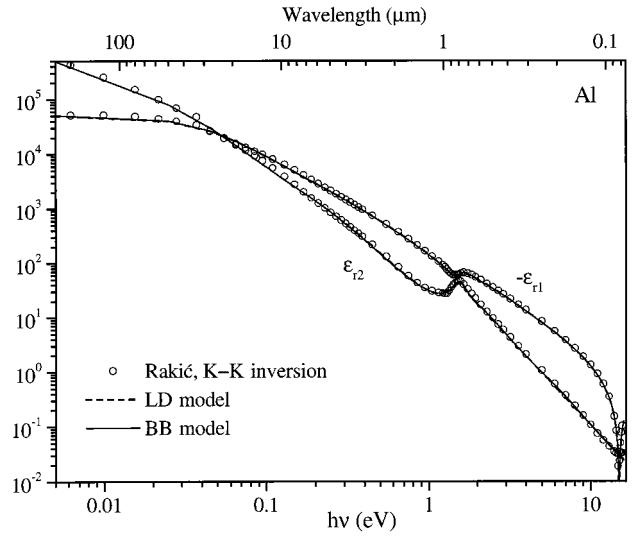

Fig. 4. Real and imaginary parts of the optical dielectric function of Al: solid curves, values that we calculated using the BB model; dashed curves, the LD model. Also shown are selected data from Rakić.[18]

be attributed to the Gaussian broadening in the interband part of the spectrum, which becomes dominant in this region.

C. Copper

Data for the copper that we used in this research are from the studies of Hagemann *et al.*[50] and Ordal *et al.*[26] The composite data set reported in Ref. 50 was obtained by combining original transmission measurements, performed on films evaporated in the conventional vacuum, with data from various sources[36,51–53] to provide an absorption spectrum large enough for a K–K analysis. Results of this analysis are tabulated in Refs. 45 and 25. The data of Ordal *et al.*,[26] pertinent in the IR and far-IR range, are obtained from the K–K analysis of their reflectance data. We used the data of Ordal *et al.*[26] from 0.1 to 0.87 eV and data of Hagemann *et al.*[50] from 1 to 6 eV. Figure 3 depicts the real and the imaginary part of the dielectric function as a function of energy (open circles, tabulated data; solid curves, the BB model; dashed curves, the LD model).

An interesting new result is the surface plasmon–polariton study of Nash and Sambles.[54] They thermally deposited copper film, 350 nm thick, onto the high-quality silica grating with a well-defined pitch (800 nm) and a profile. Film was covered by a 50-nm-thick layer of silicon monoxide without being removed from vacuum. In Fig. 3 we compare several experimental data sets for Cu, showing that the values of Nash and Sambles for ϵ_{r1} closely agree with the data of Hagemann *et al.*[50] and Ordal *et al.*[26] in the region of overlap. The values of Nash and Sambles for $\epsilon_{r2}(\omega)$ are smaller than the majority of other data in the visible range; authors have claimed that this is due to the absence of contamination in their protected copper films.[54]

D. Aluminum

To fit the models to data for Al we used results from a recent study of Rakić.[18] In Ref. 18 optical and electron-energy-loss data for evaporated aluminum films have been critically analyzed and used in an iterative, self-consistent algorithm presenting the combination of the K–K analysis and the LD model application. New values for the optical functions of aluminum have been reported in the wide spectral range from 200 μm (6.2 meV) to 0.12 nm (10 keV). These functions are in accordance with recent calculations of Lee and Chang,[55] dc conductivity measurements, and are in good agreement with both the peak position and the linewidth of the electron-energy-loss data. The results are examined for internal consistency by inertial and *f*-sum rules. Figure 4 shows excellent agreement between tabulated data[18] (open circles) and models (solid curves, BB model; dashed curves, LD model). Recent research of Nguyen *et al.*[56] shows that for high-rate-evaporated aluminum the electron mean free path increases by nearly an order of magnitude over the thickness range of 5.5–6 nm, representing a transition of the particle film in the continuous film with single-crystalline grains that span the thickness of the film. For thicknesses over the 6-nm parallel-band, transitions that dominate the bulk-material interband spectrum are noticeable. Keeping in mind that aluminum layers used in optoelectronic devices are usually more than 10 nm thick, we expect the bulk dielectric function of aluminum presented here to be a reasonably good approximation for aluminum thin-film dielectric function.

E. Beryllium

There have been only a few studies of optical properties of Be, and they produced different results, espe-

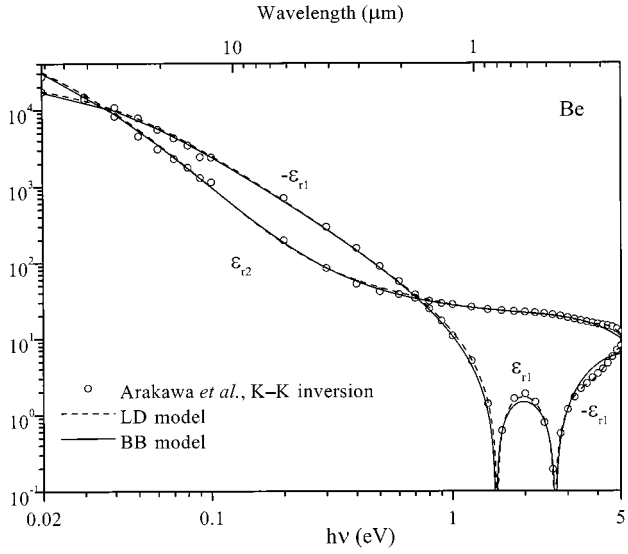

Fig. 5. Real and imaginary parts of the optical dielectric function of Be versus photon energy (open circles, data from Arakawa *et al.*[57]; solid curves, the BB model; dashed curves, the LD model).

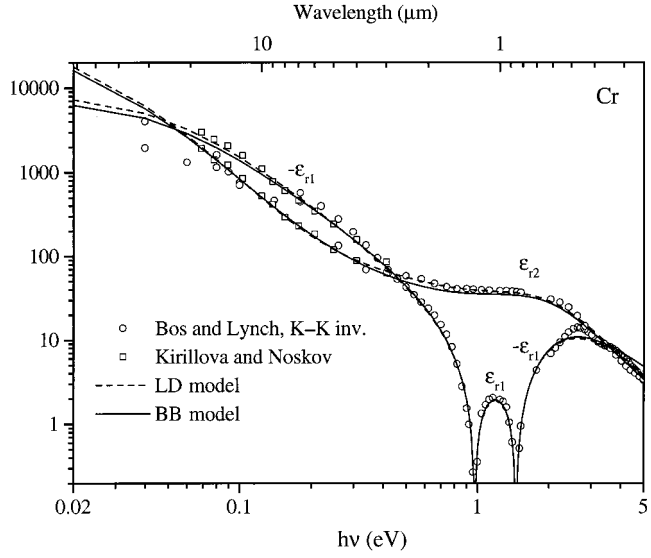

Fig. 6. Real and imaginary parts of the optical dielectric function of Cr: solid curves, values that we calculated using the BB model; dashed curves, the LD model. Also shown are tabulated data from Bos and Lynch[58] and Kirillova and Noskov.[60]

cially in the visible range of the spectrum. The inconsistency in the results can be attributed to the difficulty of sample preparation. The data that we used for fitting are from the excellent study of Arakawa *et al.*[57] They obtained a consistent set of optical constants by performing a K–K analysis in the wide spectral range from 0.06 to 26 eV, using normal-incidence reflectance data from various sources. Figure 5 shows the real and the imaginary part of the optical dielectric function as a function of energy. Open circles represent data from Ref. 57; the solid curves, the BB model; and the dashed curves, the LD model.

F. Chromium

In our research we used the K–K-analysis data of Bos and Lynch,[58] tabulated in Ref. 59, and the bulk-sample ellipsometric data of Kirillova and Noskov,[60] tabulated in Ref. 29. The measurements of Bos and Lynch[58] extend to 0.095 eV in the IR, although their K–K analysis extends further. We used their data between 0.46 and 5 eV. Kirillova and Noskov[60] reported measurements in the 0.069–4.9-eV range. We used their data between 0.069 and 0.41 eV.

The frequently quoted data of Johnson and Christy,[61] measured in the 0.64–6.60-eV range, show lower reflectance values, probably due to the fine-grain structure and voids in the films. One result of their research, which is particularly important to our application, addresses the change in optical constants with film thickness. The optical constants of Cr measured on two films, with thicknesses of 40 and 50 nm, agreed with each other well within the estimated experimental error.[61] However, measurements on 36- and 26-nm-thick films showed a slight increase in n with decreasing film thickness, whereas the value of k was almost unaffected. Figure 6 shows our calculated values for the real and the imaginary part of the dielectric function of chromium. Good agreement with experimental data can be observed for both models.

G. Nickel

Nickel does not behave as a free-electron metal for wavelengths shorter than ~20 μm; probably because of this agreement among the published optical functions of Ni is good. Here we used data from the research of Lynch and Hunter.[45] This consistent set of optical functions is obtained by K–K inversion of reflectance and absorptance data from a number of sources in the range from 0.08 to 50 eV. For our fits we have employed data from 0.2 to 5 eV. Figure 7 shows the real and the imaginary part of the optical dielectric function versus photon energy (open circles, tabulated data; solid curves, BB model; dashed curves, LD model). Good agreement between tabulated data and both models can be observed.

H. Palladium

The optical properties of palladium have been the subject of several investigations. Unfortunately, results disagree as to the magnitude of the optical functions, depending strongly on sample preparation and the method for the analysis of experimental data.

In this paper we used the data from Weaver and Benbow[62] in the 0.1–0.6-eV range and from Johnson and Christy[61] between 0.6 and 6 eV. These data are also tabulated in the review of Borghesi and Piaggi.[63] Johnson and Christy[61] reported the systematic dependence of optical constants on film thickness. Analyzing films 16.7, 25.2, 32.4, and 41.2 nm thick, they noted that the values of the conductivities increased with film thickness. In the case of the three thickest films, the successive differences were not more than the assumed experimental error. This indicates

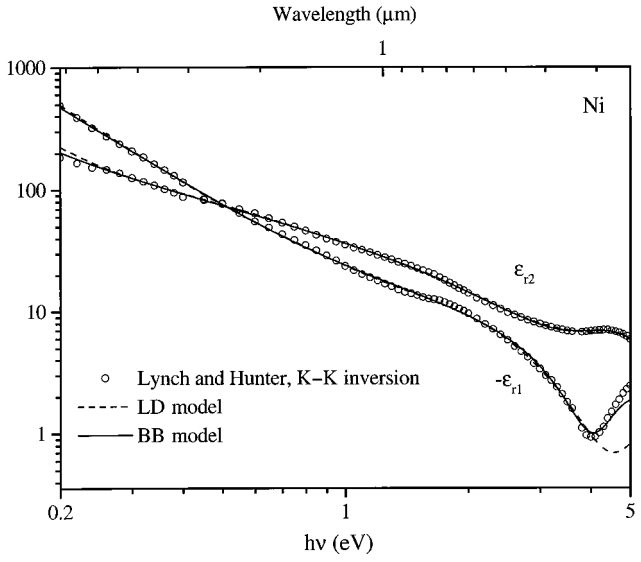

Fig. 7. Real and imaginary parts of the optical dielectric function of Ni: solid curves, values that we calculated using the BB model; dashed curves, the LD model. Also shown are tabulated data from Lynch and Hunter.[45]

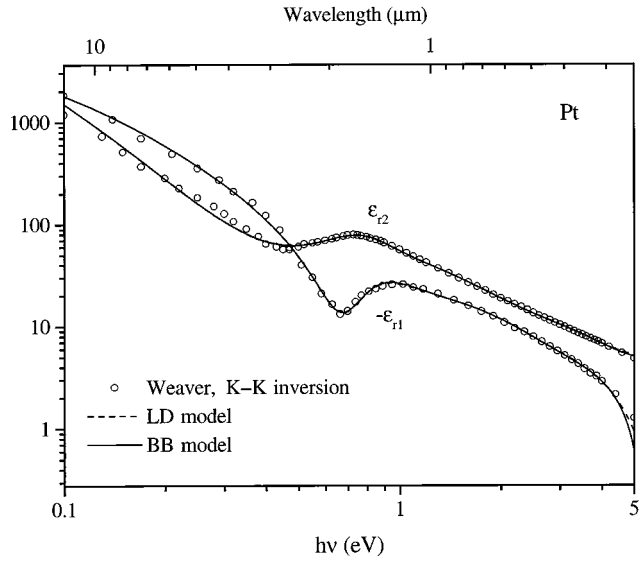

Fig. 9. Real and imaginary parts of the optical dielectric function of Pt versus photon energy (open circles, data from Weaver[64]; solid curves, BB model; dashed curves, LD model).

that, for thicknesses of more than 20 nm, bulklike values of optical constants represent a good approximation. Figure 8 shows excellent agreement between our fits (for both models) and tabulated values of the real and the imaginary part of the optical dielectric function.

I. Platinum

To fit our model to data, we used the tabulation of the optical constants of Pt given in 45 based on the study of Weaver.[64] Weaver used reflectance[65–67] and transmittance[68] data from a number of sources to obtain n and k by the K–K technique. Interband transitions for platinum are expected, according to Ref. 69, at ~6.3, 7.8, 9.3, and 10.8 eV. The structure of optical constants[64] is evident at approximately 7.4 and 9.8 eV. As the other transition metals do, platinum possesses the characteristic minimum in ϵ_{r2} with an additional structure at higher energy. Figure 9 shows a dielectric function versus energy for platinum (open circles, tabulated data; solid curves, BB model; dashed curves, LD model).

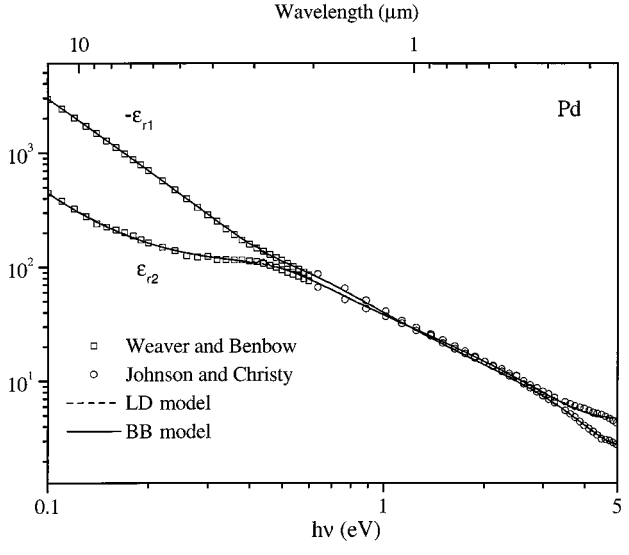

Fig. 8. Real and imaginary parts of the optical dielectric function of Pd: solid curves, values that we calculated using the BB model; dashed curves, the LD model. Also shown are tabulated data from Weaver and Benbow[62] and Johnson and Christy.[61]

J. Titanium

Johnson and Christy[61] investigated the reflectivity and the transmissivity of thin titanium films (29.8–35 nm thick) evaporated in a conventional vacuum from a tungsten filament. A fast evaporation rate was used to insure the surface smoothness of the films. Lynch *et al.*[70] reported reflectivity and absorptivity measurements of mechanically polished and electropolished bulk Ti samples in the energy range from 0.1 to 30 eV. K–K analysis was used to invert the measured spectrum to the optical dielectric function. This data set is tabulated in Ref. 71 (pp. 12–145), but owing to an error, instead of Ref. 70 the paper by Johnson and Christy[61] is quoted as a source of data. Kirillova and coworkers[72–74] used an ellipsometric technique to measure the optical constants of mechanically and chemically polished polycrystalline samples from 0.06 to 2.6 eV.

The ϵ_{r1} values from Kirillova and coworkers are in reasonably good agreement with the data of Johnson and Christy[61] in the region of overlap, although all the energies of the structures do not agree well. The ϵ_{r2} values from Kirillova and coworkers are noticeably lower (for photon energies greater than 1 eV). The prominent maximum in the ϵ_{r1} values of Lynch *et al.*[70] at ~0.46 eV is absent in the data of Kirillova and coworkers.[72–74] The weaker peak in the ϵ_{r1} values of

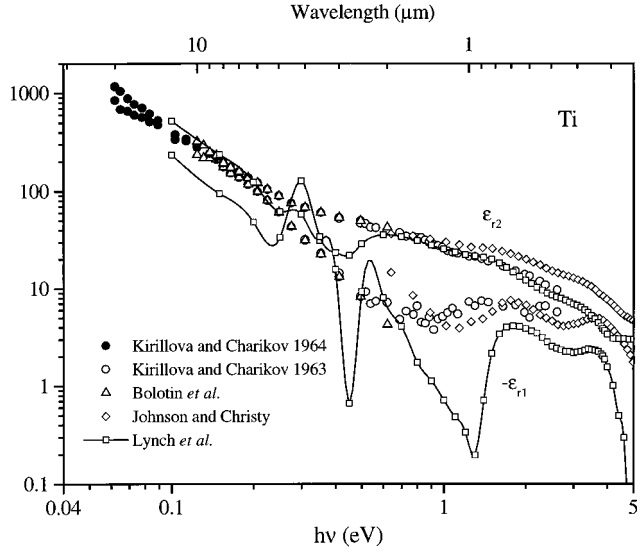

Fig. 10. Real and imaginary parts of the optical dielectric function of Ti: experimental data points, Kirillova and Charikov,[72,73] Bolotin *et al.*,[74] Johnson and Christy,[61] and Lynch *et al.*[70]

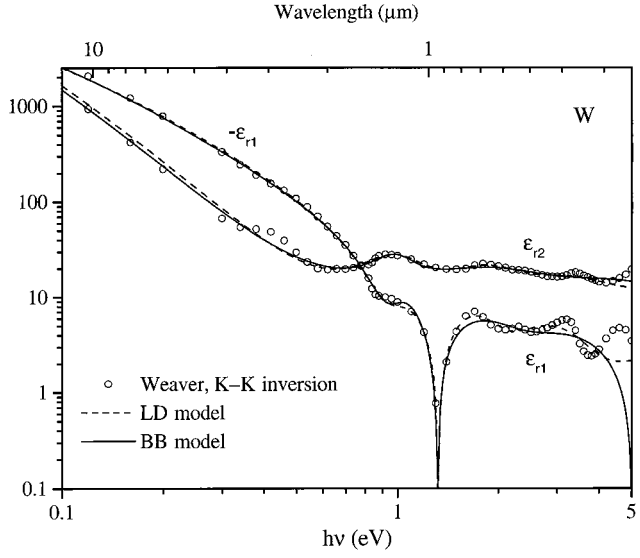

Fig. 12. Real and imaginary parts of the optical dielectric function of W versus photon energy (open circles, data from Weaver *et al.*[75]; solid curves, BB model; dashed curves, LD model).

Lynch *et al.*[70] located at 1.3 eV can be noticed in the data of Johnson and Christy[61] at ~1.15 eV and in the data of Kirillova and coworkers at ~1 eV (see Fig. 10).

In our fits we used data from Kirillova and Charikov[72,73] in the energy range from 0.06 to 2.6 eV. In Fig. 11 we compare the real and the imaginary part of the model dielectric function of Ti against the pertinent experimental data.

K. Tungsten

Most measurements of the optical functions of tungsten are in good agreement. In this paper we used the optical constants of Weaver *et al.*[75] tabulated in Ref. 45. Optical constants were obtained by the K–K inversion of reflectivity data in combination with the absorption spectrum from Haensel *et al.*[68] Figure 12 shows the real and the imaginary part of the dielectric function of W versus photon energy (open circles, tabulated data; solid curves, BB model; dashed curves, LD model).

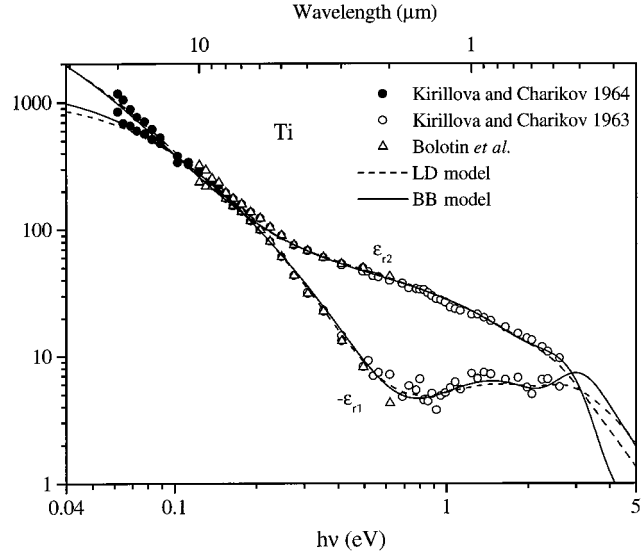

Fig. 11. Real and imaginary parts of the optical dielectric function of Ti: solid curves, values that we calculated using the BB model; dashed curves, the LD model. Also shown are tabulated data from Kirillova and Charikov[72,73] and Bolotin *et al.*[74]

4. Comparisons and Conclusions

If one treats a metal as a perfect conductor, one needs only to enforce the tangential component of the electric field $E_{\tan} = 0$ on its surface since there is no field penetration into it. Material response is π out of phase with respect to the electric field incident on the metal. This phase difference of a half-period is a delay between the time when the incident field is absorbed and the time when it is reradiated by the medium. Interference between these two fields causes the high reflectivity of the metal. In the IR and visible wavelength range, the phase change on reflection from real metal is always less than π and can be strongly frequency dependent in the vicinity of the interband transition frequencies. Consequently, the reflectivity R is also less than one. To illustrate this we calculated $R(\omega)$ and $\varphi(\omega)$ for four semiconductor–metal interfaces in the spectral range from 0.1 to 6 eV (12.4–0.2 μm). We employed models for the optical constants of metals [$N(\omega) = n(\omega) - ik(\omega)$] described in Section 3, and for GaAs we used our model for $N(\omega) = n(\omega) - ik(\omega)$ described in Ref. 76. Figure 13 shows reflectivities for GaAs–Ag, GaAs–Au, GaAs–Al, and GaAs–Pt interfaces. Figure 14 depicts the phase change on reflection for the same four interfaces in the same wavelength range.

Let us now compare the DBR mirror terminating on air [Fig. 15(a)] and the one terminating on a metallic layer [Figs. 15(b) and 15(c)]. If the semiconductor layers comprising the DBR are of a quarter-

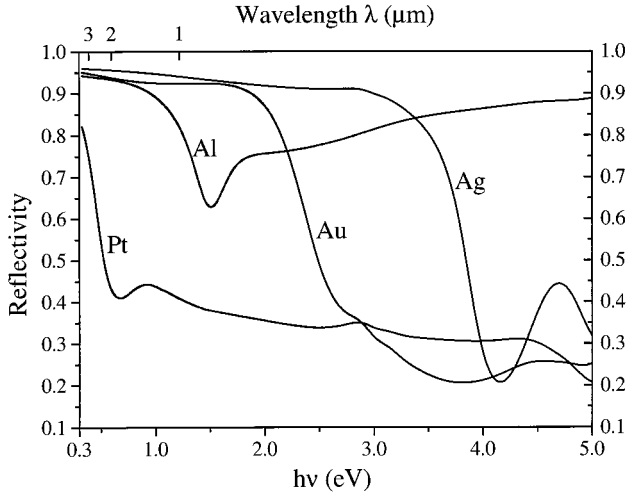

Fig. 13. Calculated reflectivities for four GaAs–metal interfaces: GaAs/100 nm Ag, GaAs/100 nm Au, GaAs/100 nm Al, and GaAs/100 nm Pt.

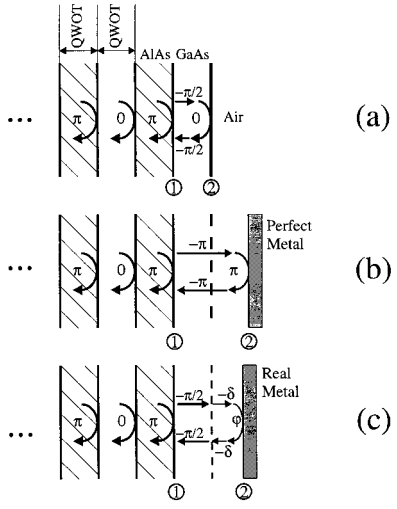

Fig. 15. DBR mirror terminating on (a) air, (b) perfectly conductive metal, and (c) real metal.

wave optical thickness (QWOT), the wave reflected from interface 1, which undergoes the phase change on reflection $\varphi = \pi$ [see Fig. 15(a)], is in phase with the wave reflected from interface 2, which experiences a phase shift $\delta = -\pi$ while making a round trip through the last high-index layer (GaAs) and no phase change on reflection. The additional high-index QWOT layer (the phase-matching layer) is needed between the last semiconductor layer and the perfectly conductive metallic layer [see Fig. 15(b)] to keep the waves reflected from interfaces 1 and 2 in phase. Therefore the round-trip phase shift $-\pi$ in the phase-matching layer cancels the phase change on reflection at the semiconductor–metal interface, $\varphi = \pi$. If we now consider the real metal with the complex refractive index $N = n - ik$, the phase change on reflection φ is determined by Eq. (14), where $\varphi < \pi$ at all wavelengths. To keep the waves reflected from interfaces 1 and 2 in phase, one needs to have a matching layer with phase thickness δ satisfying $-2\delta + \varphi = 0$ [see Fig. 15(c)]. Therefore the required phase thickness of the phase-matching layer is

$$\delta = \frac{\varphi}{2} = \frac{2\pi}{\lambda_0} nd, \tag{16}$$

where λ_0 is the vacuum wavelength, while n and d are the refractive index and the physical thickness of the phase-matching layer. The needed thickness d is therefore

$$d = \frac{\varphi}{\pi}\left(\frac{\lambda_0}{4n}\right) = \frac{\varphi}{\pi}\,(\text{QWOT}). \tag{17}$$

It is important therefore that we know precisely the phase change on reflection from the metal–semiconductor interface (φ) to be able to calculate the thickness of the phase-matching layer. A recent paper of Babić *et al.*[77] describes a method for direct measurement of φ that uses the specifically designed cavity. They recorded the reflectance spectra of Fabry–Perot (F–P) resonators formed by semiconductor layers clad by (a) air on one side and a dielectric on the other and (b) air on one side and a metal multilayer on the other. Reference 77 presents the measured reflectance for two F–P cavities: (a) air–GaAs (1000 nm)–wax and (b) air–GaAs (1000 nm)–Ti/Au (2 nm/170 nm)–wax. We used a transfer-matrix method to calculate the reflectivity of structures (a) and (b). Results are depicted in Fig. 16. Again, for the optical constants of metals we used the models from Section 3 and for the GaAs model described in Ref. 76. The solid curves are from the transfer-matrix calculations; the dashed curves show the experimental data from 77. The phase change on reflection at 1550 nm estimated from the experiment ($\varphi_{\text{exp}} \approx 137°$) is in accordance with our calculated phase $\varphi_{\text{calc}} = 139°$.

In this paper we present, for the first time to our

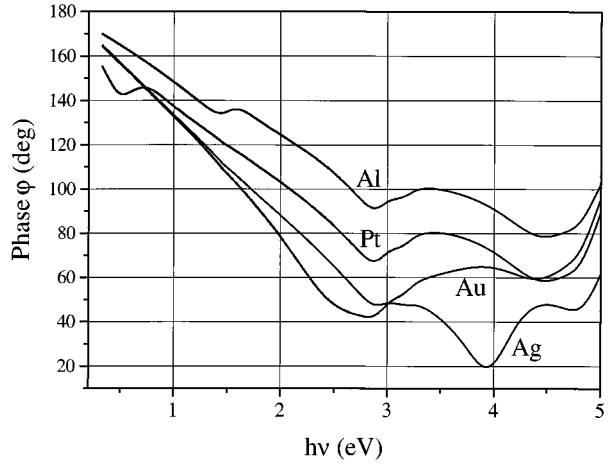

Fig. 14. Calculated phase changes on reflection for four GaAs/metal interfaces: GaAs/100 nm Ag, GaAs/100 nm Au, GaAs/100 nm Al, and GaAs/100 nm Pt.

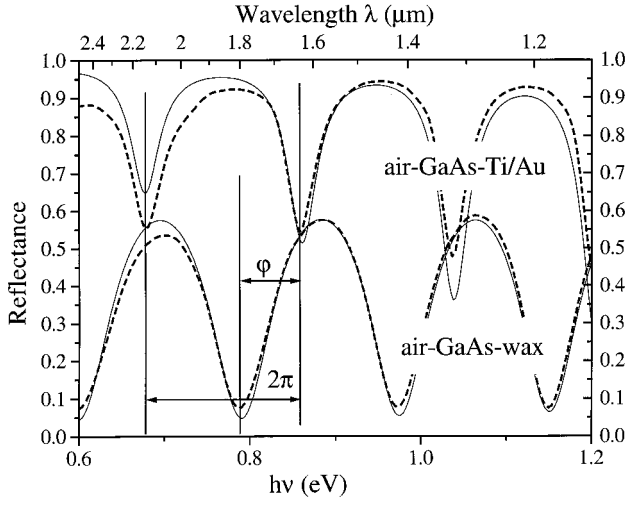

Fig. 16. Measured and calculated reflectivity of metal clad (air–GaAs–Ti/Au) and dielectric clad (air–GaAs–wax) F–P cavities: reflectance that we calculated using the transfer matrix method, solid curves; experimental curves from Ref. 77, dashed curves.

knowledge, a comprehensive parameterization of the optical functions for 11 metals for applications in optoelectronic and optical devices: noble metals (Ag, Au, and Cu), aluminum, beryllium, and some of the transition metals (Cr, Ni, Pd, Pt, Ti, and W). We used two simple phenomenological models, namely, the LD and the BB models to interpret both the free-electron and the interband parts of the dielectric response of real metals in the wide spectral range from 0.1 to 6 eV. Our results show that the BB model was needed for an appropriate description of the onset of interband absorption in noble metals (Ag, Au, Cu), while for aluminum and the transition metals both models exhibit good agreement with the experimental data. This is in accordance with our initial assumptions. The LD model due to the extended absorption of the Lorentz oscillators can hardly describe a sharp absorption edge, unless a large number of oscillators were used to describe that transition. In such a case it is physically justified and computationally simpler to employ a single Gaussian-like BB oscillator instead.

Although it is known that the optical constants of thick films (bulk) can differ from the optical constants of thin metallic films, the optical constants of evaporated films still provide a good approximation. For all the metals we carefully chose relevant optical data, trying always to use the measurements obtained on films similar (in terms of geometry, morphology, and the growth process) to the films used in optoelectronic devices. Comparison with the measurements on surface normal structures confirmed that the reflectance and the phase change on reflection from semiconductor–metal interfaces (including the case of metallic multilayers) can be accurately calculated by use of the proposed models for the optical functions of metals and the transfer matrix theory.

Appendix A

The Brendel–Borman model requires the integration of Eq. (4) in closed form. The integral to be solved is

$$\chi_j(\omega) = \frac{1}{\sqrt{2\pi}\sigma_j}\int_{-\infty}^{+\infty}\exp\left[-\frac{(x-\omega_j)^2}{2\sigma_j^2}\right] \times \frac{f_j{\omega_p}^2}{(x^2-\omega^2)+i\omega\Gamma_j}\,\mathrm{d}x. \tag{A1}$$

We define ${a_j}^2 = \omega^2 - i\Gamma_j\omega$ with $\mathrm{Im}[a_j] > 0$ and obtain

$$\chi_j(\omega) = -\frac{f_j{\omega_p}^2}{\sqrt{2\pi}\sigma_j}\int_{-\infty}^{+\infty}\frac{\exp\left[-\frac{(x-\omega_j)^2}{2\sigma_j^2}\right]}{a_j^2-x^2}\,\mathrm{d}x, \tag{A2}$$

$$\chi_j(\omega) = -\frac{f_j{\omega_p}^2}{2\sqrt{2\pi}a_j\sigma_j}\left\{\int_{-\infty}^{+\infty}\frac{\exp\left[-\frac{(x-\omega_j)^2}{2\sigma_j^2}\right]}{a_j-x}\,\mathrm{d}x + \int_{-\infty}^{+\infty}\frac{\exp\left[-\frac{(x-\omega_j)^2}{2\sigma_j^2}\right]}{a_j+x}\,\mathrm{d}x\right\}. \tag{A3}$$

Now the first integral can be written as

$$I_1 = \int_{-\infty}^{+\infty}\frac{\exp\left[-\frac{(x-\omega_j)^2}{2\sigma_j^2}\right]}{(a_j-\omega_j)-(x-\omega_j)}\,\mathrm{d}x. \tag{A4}$$

By introducing $t = (x-\omega_j)/(\sqrt{2}\sigma_j)$ and $z_1 = (a_j-\omega_j)/(\sqrt{2}\sigma_j)$, we find that [see Ref. 41, Eqs. (7.1.3) and (7.1.4)]

$$I_1 = \int_{-\infty}^{+\infty}\frac{e^{-t^2}}{z_1-t}\,\mathrm{d}t = \frac{\pi}{i}\,e^{-{z_1}^2}\,\mathrm{erfc}(-iz_1) = \frac{\pi}{i}\,w\left(\frac{a_j-\omega_j}{\sqrt{2}\sigma_j}\right). \tag{A5}$$

Using a similar approach, we can solve the second integral

$$I_2 = \int_{-\infty}^{+\infty}\frac{\exp\left[-\frac{(x-\omega_j)^2}{2\sigma_j^2}\right]}{(a_j-\omega_j)+(x-\omega_j)}\,\mathrm{d}x \tag{A6}$$

by introducing $t = (x-\omega_j)/(\sqrt{2}\sigma_j)$ and $z_2 = (a_j+\omega_j)/(\sqrt{2}\sigma_j)$:

$$I_2 = \int_{t=-\infty}^{t=+\infty}\frac{e^{-t^2}}{z_2+t}\,\mathrm{d}t = \int_{t=-\infty}^{t=+\infty}\frac{e^{-t^2}}{z_2-t}\,\mathrm{d}t = \frac{\pi}{i}\,e^{-{z_2}^2}\,\mathrm{erfc}(-iz_2) = \frac{\pi}{i}\,w\left(\frac{a_j+\omega_j}{\sqrt{2}\sigma_j}\right). \tag{A7}$$

If Eqs. (A5) and (A7) are finally substituted into Eq. (A1), we obtain the result

$$\chi_j = \frac{i\sqrt{\pi}\, f_j {\omega_p}^2}{2\sqrt{2}a_j\sigma_j}\left[w\left(\frac{a_j-\omega_j}{\sqrt{2}\sigma_j}\right)+w\left(\frac{a_j+\omega_j}{\sqrt{2}\sigma_j}\right)\right]. \quad \text{(A8)}$$

References

1. R. S. Geels, S. W. Corzine, and L. A. Coldren, "InGaAs vertical-cavity surface-emitting lasers," IEEE J. Quantum Electron. **27,** 1359–1367 (1991).
2. C. J. Chang-Hasnain, J. B. Harbison, G. Hasnain, A. C. Von Lehmen, L. T. Florez, and N. G. Stoffel, "Dynamic, polarization, and transverse mode characteristics of vertical cavity surface emitting lasers," IEEE J. Quantum Electron. **27,** 1402–1409 (1991).
3. K. Iga, "Surface emitting lasers," Opt. Quant. Electron. **24**(2), s97–s104 (1992).
4. T. Baba, R. Watanabe, K. Asano, F. Koyama, and K. Iga, "Theoretical and experimental estimations of photon recycling effect in light emitting devices with a metal mirror," Jpn. J. Appl. Phys. **35**(1A), 97–100 (1996).
5. G. Du, K. A. Stair, G. Devane, J. Zhang, R. P. H. Chang, C. W. White, X. Li, Z. Wang, and Y. Liu, "Vertical-cavity surface-emitting laser with a thin metal mirror fabricated by double implantation using a tungsten wire mask," Semicond. Sci. Technol. **11,** 1734–1736 (1996).
6. G. M. Smith, D. V. Forbes, R. M. Lammert, and J. J. Coleman, "Metalization to asymetric cladding separate confinement heterostructure lasers," Appl. Phys. Lett. **67,** 3847–3849 (1995).
7. C. H. Wu, P. S. Zory, and M. A. Emanuel, "Contact reflectivity effects on thin *p*-clad InGaAs single quantum-well lasers," IEEE Photon. Technol. Lett. **6,** 1427–1429 (1994).
8. H. J. Luo and P. S. Zory, "Distributed feedback coupling coefficient in diode lasers with metallized gratings," IEEE Photon. Technol. Lett. **2,** 614–616 (1990).
9. E. Hadji, J. Bleuse, N. Magnes, and J. L. Pautrat, "3.2-μm infrared resonant cavity light emitting diode," Appl. Phys. Lett. **67,** 2591–2593 (1995).
10. N. E. J. Hunt, E. F. Schubert, R. F. Kopf, D. L. Sivco, A. Y. Cho, and G. J. Zydzik, "Increased fiber communications bandwidth from a resonant cavity light emitting diode emitting at $\lambda = 940$ nm," Appl. Phys. Lett. **63,** 2600–2602 (1993).
11. E. F. Schubert, Y.-H. Wang, A. Y. Cho, L.-W. Tu, and G. J. Zydzik, "Resonant cavity light-emitting diode," Appl. Phys. Lett. **60,** 921–923 (1992).
12. B. Corbett, L. Considine, S. Walsh, and W. M. Kelly, "Resonant cavity light emitting diode and detector using epitaxial liftoff," IEEE Photon. Technol. Lett. **5,** 1041–1043 (1993).
13. S. T. Wilkinson, N. M. Jokerst, and R. P. Leavitt, "Resonant-cavity-enhanced thin-film AlGaAs/GaAs/AlGaAs LED's with metal mirrors," Appl. Opt. **34,** 8298–8302 (1995).
14. B. Corbett, L. Considine, S. Walsh, and W. M. Kelly, "Narrow bandwidth long wavelength resonant cavity photodiodes," Electron. Lett. **29,** 2148–2149 (1993).
15. M. S. Ünlü and S. Strite, "Resonant cavity enhanced photonic devices," J. Appl. Phys. **78,** 607–639 (1995).
16. A. Katz, "Physical and chemical deposition of metals as ohmic contacts to InP and related materials," in *Handbook of Compound Semiconductors*, P. H. Holloway and G. E. McGuire, eds. (Noyes Publications, Park Ridge, N.J., 1995), pp. 170–250.
17. L. Yang, M. C. Wu, K. Tai, T. Tanbun-Ek, and R. A. Logan, "InGaAsP(1.3-μm)/InP vertical-cavity surface-emitting laser grown by metalorganic vapor phase epitaxy," Appl. Phys. Lett. **56,** 889–891 (1990).
18. A. D. Rakić, "Algorithm for the determination of intrinsic optical constants of metal films: application to aluminum," Appl. Opt. **34,** 4755–4767 (1995).
19. N. W. Ashcroft and K. Sturm, "Interband absorption and the optical properties of polyvalent metals," Phys. Rev. B **3,** 1898–1910 (1971).
20. C. J. Powell, "Analysis of optical and inelastic-electron-scattering data II. Application to Al," J. Opt. Soc. Am. **60,** 78–93 (1970).
21. M. Erman, J. B. Theeten, P. Chambon, S. M. Kelso, and D. E. Aspnes, "Optical properties and damage analysis of GaAs single crystals partly amorphized by ion implantation," J. Appl. Phys. **56,** 2664–2671 (1984).
22. C. M. Herzinger, H. Yao, P. G. Snyder, F. G. Celii, Y. C. Kao, B. Johs, and J. A. Woollam, "Determination of AlAs optical constants by variable-angle spectroscopic ellipsometry and a multisample analysis," J. Appl. Phys. **77,** 4677–4687 (1995).
23. M. Schubert, V. Gottschalch, C. M. Herzinger, H. Yao, P. G. Snyder, and J. A. Woollam, "Optical-constants of $Ga_xIn_{1-x}P$ lattice-matched to GaAs," J. Appl. Phys. **77,** 3416–3419 (1995).
24. C. M. Herzinger, P. G. Snyder, F. G. Celii, Y. C. Kao, D. Chow, B. Johs, and J. A. Woollam, "Studies of thin strained InAs, AlAs, and AlSb layers by spectroscopic ellipsometry," J. Appl. Phys. **79,** 2663–2674 (1996).
25. M. A. Ordal, L. L. Long, R. J. Bell, S. E. Bell, R. R. Bell, Jr., R. W. Alexander, and C. A. Ward, "Optical properties of the metals Al, Co, Cu, Au, Fe, Pb, Ni, Pd, Pt, Ag, Ti, and W in the infrared and far infrared," Appl. Opt. **22,** 1099–1119 (1983).
26. M. A. Ordal, R. J. Bell, R. W. Alexander, Jr., L. L. Long, and M. R. Querry, "Optical properties of fourteen metals in the infrared and far infrared: Al, Co, Cu, Au, Fe, Pb, Mo, Ni, Pd, Pt, Ag, Ti, V, and W," Appl. Opt. **24,** 4493–4499 (1985).
27. E. D. Palik, ed., *Handbook of Optical Constants of Solids I* (Academic, Orlando, Fla., 1985).
28. E. D. Palik, ed., *Handbook of Optical Constants of Solids II* (Academic, San Diego, Calif., 1991).
29. C. L. Foiles, "Optical properties of pure metals and binary alloys," in *Landolt-Börnstein, Group III: Crystal and Solid State Physics*, K.-H. Hellwege and O. Madelung, eds., Vol. 15b of New Series (Springer-Verlag, Berlin, 1985), Chap. 4, pp. 210–489.
30. L. Ward, *The Optical Constants of Bulk Materials and Films*, The Adam Hilger Series on Optics and Optoelectronics (Adam Hilger, Bristol, UK, 1988).
31. R. Brendel and D. Bormann, "An infrared dielectric function model for amorphous solids," J. Appl. Phys. **71,** 1–6 (1992).
32. A. D. Rakić, J. M. Elazar, and A. B. Djurišić, "Acceptance-probability-controlled simulated annealing: a method for modeling the optical constants of solids," Phys. Rev. E **52,** 6862–6867 (1995).
33. A. B. Djurišić, J. M. Elazar, and A. D. Rakić, "Modeling the optical constants of solids using genetic algorithms with parameter space size adjustment," Opt. Commun. **134,** 407–414 (1997).
34. A. B. Djurišić, A. D. Rakić, and J. M. Elazar, "Modeling the optical constants of solids using acceptance-probability-controlled simulated annealing with an adaptive move generation procedure," Phys. Rev. E **55,** 4797–4803 (1997).
35. H. Ehrenreich, H. R. Philipp, and B. Segall, "Optical properties of aluminum," Phys. Rev. **132,** 1918–1928 (1963).
36. H. Ehrenreich and H. R. Philipp, "Optical properties of Ag and Cu," Phys. Rev. **128,** 1622–1629 (1962).
37. M. I. Marković and A. D. Rakić, "Determination of the reflection coefficients of laser light of wavelengths $\lambda \in (0.22\ \mu\text{m}, 200\ \mu\text{m})$ from the surface of aluminum using the Lorentz–Drude model," Appl. Opt. **29,** 3479–3483 (1990).
38. M. I. Marković and A. D. Rakić, "Determination of optical properties of aluminum including electron reradiation in the Lorentz–Drude model," Opt. Laser Technol. **22,** 394–398 (1990).

39. C. C. Kim, J. W. Garland, H. Abad, and P. M. Raccah, "Modeling the optical dielectric function of semiconductors: extension of the critical-point parabolic-band approximation," Phys. Rev. B **45,** 11,749–11,767 (1992).
40. C. C. Kim, J. W. Garland, and P. M. Raccah, "Modeling the optical dielectric function of the alloy system $Al_xGa_{1-x}As$," Phys. Rev. B **47,** 1876–1888 (1993).
41. M. Abramowitz and I. A. Stegun, eds., *Handbook of Mathematical Functions* (Dover, New York, 1972).
42. S. Wolfram, *The Mathematica Book*, 3rd ed. (Wolfram Media/Cambridge U. Press, Cambridge, UK, 1996).
43. H. A. Macleod, *Thin-Film Optical Filters* (Adam Hilger, Bristol, UK, 1986).
44. Z. Knittl, *Optics of Thin Films* (Wiley, New York, 1976).
45. D. W. Lynch and W. R. Hunter, "Comments on the optical constants of metals and an introduction to the data for several metals," in *Handbook of Optical Constants of Solids*, E. D. Palik, ed. (Academic, Orlando, Fla., 1985), pp. 275–367.
46. B. Dold and R. Mecke, "Optische Eigenschaften von Edelmetallen, Übergangsmetallen und deren Legierungen im Infrarot (1. Teil)," Optik **22,** 435–446 (1965).
47. P. Winsemius, H. P. Langkeek, and F. F. van Kampen, "Structure dependence of the optical properties of Cu, Ag and Au," Physica **79B,** 529–546 (1975).
48. G. Leveque, C. G. Olson, and D. W. Lynch, "Reflectance spectra and dielectric functions of Ag in the region of interband transitions," Phys. Rev. B **27,** 4654–4660 (1983).
49. M. L. Thèye, "Investigation of the optical properties of Au by means of thin semitransparent films," Phys. Rev. B **2,** 3060–3078 (1970).
50. H. J. Hagemann, W. Gudat, and C. Kunz, "Optical constants from the far infrared to the x-ray region: Mg, Al, Cu, Ag, Au, Bi, C, and Al_2O_3," J. Opt. Soc. Am. **65,** 742–744 (1975).
51. L. R. Canfield and G. Hass, "Reflectance and optical constants of evaporated copper and silver in the vacuum ultraviolet from 1000 to 2000 Å," J. Opt. Soc. Am. **55,** 61–64 (1965).
52. R. Haensel, C. Kunz, T. Sasaki, and B. Sonntag, "Absorption measurements of copper, silver, tin, gold, and bismuth in the far ultraviolet," Appl. Opt. **7,** 301–306 (1968).
53. P. B. Johnson and R. W. Christy, "Optical constants of the noble metals," Phys. Rev. B **6,** 4370–4379 (1972).
54. D. J. Nash and J. R. Sambles, "Surface plasmon-polariton study of the optical dielectric function of copper," J. Mod. Opt. **42,** 1639–1647 (1995).
55. K.-H. Lee and K. J. Chang, "First-principles study of the optical properties and the dielectric response of Al," Phys. Rev. B **49,** 2362–2367 (1994).
56. H. V. Nguyen, I. An, and R. W. Collins, "Evolution of the optical functions of thin-film aluminum: A real-time spectroscopic ellipsometry study," Phys. Rev. B **47,** 3947–3965 (1993).
57. E. T. Arakawa, T. A. Callcott, and Y.-C. Chang, "Beryllium (Be)," in *Handbook of Optical Constants of Solids II*, E. D. Palik, ed. (Academic, San Diego, Calif., 1991), pp. 421–433.
58. L. W. Bos and D. W. Lynch, "Optical properties of antiferromagnetic chromium and dilute Cr-Mn and Cr-Re alloys," Phys. Rev. B **2,** 4567–4577 (1970).
59. D. W. Lynch and W. R. Hunter, "An introduction to the data for several metals," in *Handbook of Optical Constants of Solids II*, E. D. Palik, ed. (Academic, San Diego, Calif., 1991) pp. 341–419.
60. M. M. Kirillova and M. M. Noskov, "Optical properties of chromium," Phys. Met. Metallogr. **26,** 189–192 (1968).
61. P. B. Johnson and R. W. Christy, "Optical constants of transition metals: Ti, V, Cr, Mn, Fe, Co, Ni, and Pd," Phys. Rev. B **9,** 5056–5070 (1974).
62. J. H. Weaver and R. L. Benbow, "Low-energy intraband absorption in Pd," Phys. Rev. B **12,** 3509–3510 (1975).
63. A. Borghesi and A. Piaggi, "Palladium (Pd)," in *Handbook of Optical Constants of Solids II*, E. D. Palik, ed. (Academic, San Diego, Calif., 1991), pp. 469–476.
64. J. H. Weaver, "Optical properties of Rh, Pd, Ir, and Pt," Phys. Rev. B **11,** 1416–1425 (1975).
65. A. Y.-C. Yu, W. E. Spicer, and G. Hass, "Optical properties of platinum," Phys. Rev. **171,** 834–835 (1968).
66. A. Seignac and S. Robin, "Optical properties of thin films of Pt in the far ultraviolet," Solid State Commun. **11,** 217–219 (1972).
67. G. Hass and W. R. Hunter, "New developments in vacuum-ultraviolet reflecting coatings for space astronomy," in *Space Optics*, B. J. Thompson and R. R. Shanon, eds. (National Academy of Sciences, Washington, D.C., 1974), pp. 525–553.
68. R. Haensel, K. Radler, B. Sonntag, and C. Kunz, "Optical absorption measurements of tantalum, tungsten, rhenium and platinum in the extreme ultraviolet," Solid State Commun. **7,** 1495–1497 (1969).
69. N. V. Smith, "Photoemission spectra and band structures of *d*-band metals. III. Model band calculations on Rh, Pd, Ag, Ir, Pt, and Au," Phys. Rev. B **9,** 1365–1376 (1974).
70. D. W. Lynch, C. G. Olson, and J. H. Weaver, "Optical properties of Ti, Zr, and Hf from 0.15 to 30 eV," Phys. Rev. B **11,** 3617–3624 (1975).
71. D. R. Lide, ed., *CRC Handbook of Chemistry and Physics*, 77th ed. (CRC Press, Boca Raton, Fla., 1996).
72. M. M. Kirillova and B. A. Charikov, "Study of the optical properties of transition metals," Opt. Spectrosc. USSR **17,** 134–135 (1964).
73. M. M. Kirillova and B. A. Charikov, "Optical properties of titanium in the quantum transition range," Phys. Met. Metallogr. **15,** 138–139 (1963).
74. G. A. Bolotin, A. N. Voloshinskii, M. M. Kirillova, M. M. Noskov, A. V. Sokolov, and B. A. Charikov, "Optical properties of titanium and vanadium in the infrared range of the spectrum," Phys. Met. Metallogr. **13,** 24–31 (1962).
75. J. H. Weaver, C. G. Olson, and D. W. Lynch, "Optical properties of crystalline tungsten," Phys. Rev. B **12,** 1293–1297 (1975).
76. A. D. Rakić and M. L. Majewski, "Modeling the optical dielectric function of GaAs and AlAs: extension of Adachi's model," J. Appl. Phys. **80,** 5909–5914 (1996).
77. D. I. Babić, R. P. Mirin, E. L. Hu, and J. E. Bowers, "Characterization of metal mirrors on GaAs," Electron. Lett. **32,** 319–320 (1996).